The Formation of Nanotubes and Nanocoils of Molybdenum Disulphide

V. Lavayen, [a,b,*] N. Mirabal, [b] C. O'Dwyer, [a] M. A. Santa Ana, [b] E. Benavente, [c] C. M. Sotomayor Torres, [a] G. González [b]

[a] *Tyndall National Institute, University College Cork, Cork, Ireland*

[b] *Department of Chemistry, Faculty of Science, Universidad de Chile, P. O. Box 653, Santiago, Chile*

[c] *Department of Chemistry, Universidad Tecnológica Metropolitana, P. O. Box 9845, Santiago, Chile*

Abstract

This work reports the successful realization of MoS_2 nanotubes by a novel intercalation chemistry and hydrothermal treatment. An inorganic-organic precursor of hexadecylamine (HDA) and molybdenum disulphide (MoS_2) were used in synthesizing the nanocomposite comprising laminar MoS_2 with HDA intercalated in the interlaminar spacing. The formation of MoS_2 nanotubes occurred during hydrothermal treatment (HT) by a self-organized rolling mechanism. The nanotubes were observed to have dimensions 2−12 μm in length and inner diameters typically in the range of 25−100 nm. We also report the formation of amorphous nanocoils of MoS_2 obtained during similar procedures.

Key words: Chalcogenides, Transmission electron microscopy, Molybdenum, Nanotubes, Nanostructures

1 Introduction

Since the first report of the formation of WS_2 inorganic nanotubes [1] in 1992, concentrated research efforts into synthetic methods for inorganic nanotube realization has lagged behind those for carbon nanotubes, which in the last

* Corresponding author. Tel: + 353 21 490-4391; Fax: + 353 21 490-4467.
Email address: vlavayen@tyndall.ie (V. Lavayen,).

decade has increased exponentially. Inorganic nanotube research tended to be under-investigated in the early years after their discovery [2]. The number of publications, however, reporting the synthesis of different inorganic nanotubes has increased weekly [2], revealing the importance of this field for nanotechnology. In this sense, several groups have produced inorganic nanomaterials using standard methods, e.g. Remskar et al. [3] synthesized WS_2 nanotubes using a chemical transport reaction.

In previous work by Kerridge et al. [4], KSCN and Mo were employed to synthesize MoS_2 in its melted form, but only MoS_2 of poor crystallinity was produced. In a follow up report, Zhu and co-workers [5] synthesized nanotubes and nanorods of MoS_2 by a hydrothermal method using MoO_3 and KSCN as starting materials, although the degree of uniformity distribution of the nanostructures was relatively low.

One particularly interesting compound of the chalcogenides family is molybdenum disulfide (MoS_2). This material has shown extraordinary attributes resulting in its application in a wide variety of fields such as ultra-low friction materials [6], scanning probe microscopy [7], field emission tips [8], paramagnetism [9], electrochemistry [10], hydrogen storage [11] and nanofluidics [12].

In the synthesis of these chalcogenides, several other methods were explored, e.g Rao and co-workers [13] reported MoS_2 nanotubes by simple heating of MoS_3 in a steam of hydrogen at high temperature ($\sim$1300°C), while Remskar et al. [14] employed the chemical transport method to form MoS_2 nanotubes. Multi-wall MoS_2 nanotubes have also been synthesized by an annealing process in hydrogen using needle-like tetrathiomolybdenum $(NH_4)_2MoS_4$ as a precursor. Such nanotubes were reported to allow gaseous and electrochemical storage of hydrogen [15], although their structural characterization left many open questions.

In this Communication we report the formation of molybdenum disulfide nanotubes and nanocoils using lamellar organic-inorganic compounds as precursors. This work is the first report of MoS_2 nanotube formation using organic molecule-intercalated lamellar compounds and follows on from our previous reports on the formation of nanocomposites [16,17] and nanostructures using these techniques [18,19].

2 Experimental

The method employed for the synthesis of molybdenum disulfide nanocomposite was essentially similar to that described in our previous work [20]. Molybdenum disulfide powder (particle size $<$ 2 mm) (Aldrich); Hexadecy-

lamine (HDA) 92%, *n*-butyl lithium and *n*-hexane solution (Merck) were used as received. Water was twice distilled and carefully degassed.

2.1 Synthesis of Lamellar Li_xMoS_2

Lithium intercalated molybdenum disulphide, (Li_xMoS_2, x >> 1), previously prepared by direct intercalation of lithium using *n*-butyl lithium in a 1.6 mol dm^{-3} hexane solution, is exfoliated by a 24 h moisture treatment. Amine$-MoS_2$ nanocomposites are prepared by addition of an aqueous solution of amine ($\sim 10^{-3}$ mol dm^{-3}) to the suspension of exfoliated Li_xMoS_2 (3.0×10^{-3} mol dm^{-3}), followed by stirring of the reaction mixture at 60°C for 48 h. Both hexadecylamine (HDA) and octadecylamine (ODA) were used to synthesize the nanocomposites. The resulting solid was centrifuged, washed with water and dried under vacuum.

2.2 Synthesis of MoS_2 Nanotubes

The conversion of the $Li_{0.1}MoS_2(HDA)_2$ and $Li_{0.1}MoS_2(ODA)_{2.1}$ laminar species to nanotubes was achieved by hydrothermal treatment (HT) of aqueous suspensions of the nanocomposite in a Teflon-lined autoclave in a sand bath for 12 h at 130°C.

2.3 Characterization of Samples

The morphology of the lamellar nanocomposite was examined by Scanning Electron Microscopy (SEM) using a Philips XL−30 equipped with an Energy Dispersive Spectroscopy (EDS) detector. Transmission Electron Microscopy was obtained on a JEOL 100SX operating at 100 kV. The electron diffraction of the products was obtained using the JEOL microscope internally calibrated with a gold standard (Merck, 99.99% purity; 100 kV, K = 4.614 cm Å). The diffraction patterns were obtained using a limiting field aperture (20 mm). In this way, the diffraction from the grid is avoided and the observed area is minimized. A typical SEM image of a nanocomposite product is shown in Fig. 1a, highlighting its laminar nature on the macroscopic scale. The corresponding TEM micrograph in Fig. 1b shows the morphology of an individual nanocomposite lamina.

Thermogravimetric analysis (TGA) and differential scanning calorimetry (DSC) were performed using a Perkin-Elmer Model TGA-7 Thermogravimetric system with a microprocessor driven temperature control unit and data station.

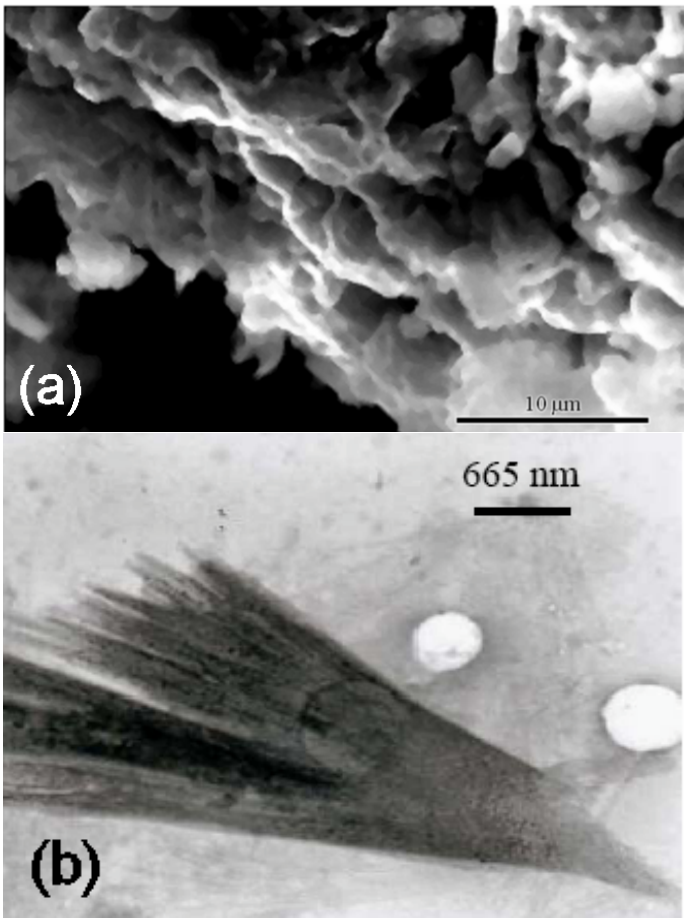

Fig. 1. (a) SEM image of the intercalation nanocomposite product $Li_{<0.1}MoS_2(ODA)_{2.1}$ (b) TEM micrograph of a single nanocomposite lamina.

The mass of the samples was generally in the 2−3 mg range. The sample was placed in the balance system equipment and the temperature was raised from 25 to 550°C at a heating rate of 10 °C min^{-1}. The mass of the sample was continuously recorded as a function of the temperature. The chemical compositions of the samples were determined by elemental chemical analysis (SISONS model EA-1108) and atomic absorption spectrometry (UNICAM 929).

3 Results and Discussion

3.1 X-ray Diffraction Analysis

The X-ray powder diffraction patterns of the pristine MoS_2 and $Li_{0.1}MoS_2$ (air exfoliated) are shown in Figs 2a and 2b, respectively. Analysis of the diffraction patterns' principal reflections for each product gives values for the interlamellar distance of 0.615 nm and 1.14 nm, respectively. These values are

in good agreement with our previous report [21].

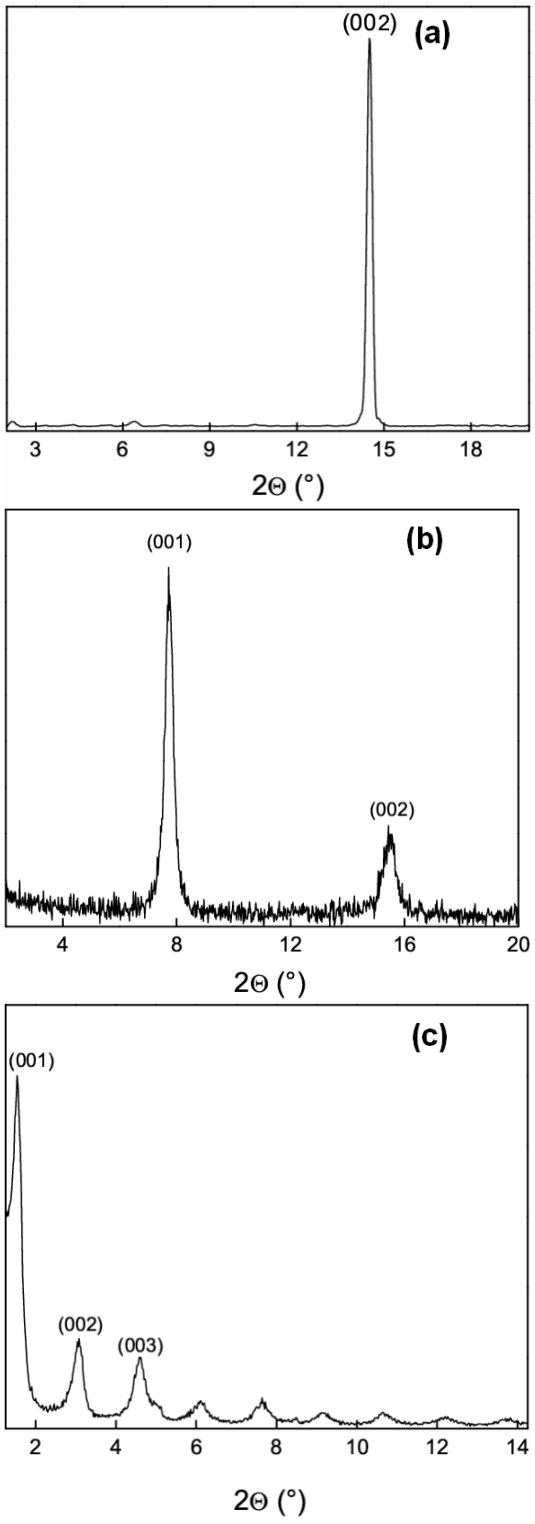

Fig. 2. X-ray patterns of each of the synthesis products (a) as-received MoS_2 (b) $Li_{0.1}MoS_2$ (air exfoliated) (c) $Li_{<0.1}MoS_2(ODA)_{2.1}$.

The diffraction pattern of the crystalline solid $Li_{0.1}MoS_2(ODA)_{2.1}$ is repro-

duced in Fig. 2c. The diffraction pattern shows the characteristics of a regular and ordered lamellar compound of the series $Li_xMoS_2(C_nH_{2n+1}NH_2)_y$, where x, y are stoichiometric coefficients. The interlamellar distance is measured to be 5.7 nm. By comparison, the compound $Li_{0.1}MoS_2(HDA)_2$ exhibits an interlaminar distance of 5.5 nm. These distances show a significant increment with respect to the value of the pristine MoS_2 and the exfoliated lithiated product due to the interlaminar presence of the long alkyl-chained amine surfactant [17].

Using X-ray diffraction techniques, it was possible to follow the intercalation process and its influence on the degree of crystallinity of the lamellar organic/inorganic nanocomposites. The diffraction pattern in Fig. 2c shows the formation of a single laminar phase in the compound. The degree of laminarity is such that the fourth order $\{00l\}$ reflections are observed. Our previous reports [16,21] of compounds intercalated with shorter length amines have only exhibited third order $\{00l\}$ reflections under similar conditions, indicating an increased order in the lithiated MoS_2 laminarity with longer chained intercalated amine surfactants.

In Fig. 2c a linear relationship is observed between the ratio of successive reflections of the $\{00l\}$ planes to that of the $\{001\}$ plane, highlighting the periodic laminar structure. The lamellar array is observed to follow a linear numerical series: $\frac{d_1}{d_1} = 1$, $\frac{d_1}{d_2} = 2$, ..., $\frac{d_1}{d_n} = n$, where d_n is the double angle position of the $\{00n\}$ reflection. This particular trend is primarily due to the presence of equidistant lamellar phases [22] and for the series of compounds $Li_xMoS_2(C_nH_{2n+1}NH_2)_y$ is caused by the equidistance between lamella with surfactant molecules arranged in a conformation with successively similar interlaminar length. The formation of these lamellar phases is typically favoured in the presence of the liquid-phase ordered assistance of the surfactant allowing for the tendency of the MoS_2 to become a lamellar structure.

Another important characteristic of such compounds based on these and previous measurements [17] is the regularity of the interlamellar distance. The amines are believed to be in a double-layer arrangement of interpenetrated alkyl chains perpendicular to the layers of the MoS_2 [20,23].

Figure 3 shows a comparison between the X−ray diffraction patterns of the post HT product (pattern **b**) to that of the lamellar precursors, HDA (pattern **c**) and MoS_2 (pattern **a**). From Fig. 3, the similarity observed in the peak positions of the amine surfactant and the post HT product infers a similarity in the phase of both compounds. This result is consistent with a segregation of the amine from the host compound. The X−ray pattern of the post−HT product does not show the presence of any particular crystalline phase of MoS_2 despite the fact that the surfactant only constitutes 14% of the total molecular weight of the organic-inorganic lamellar compound. It is not possible, however,

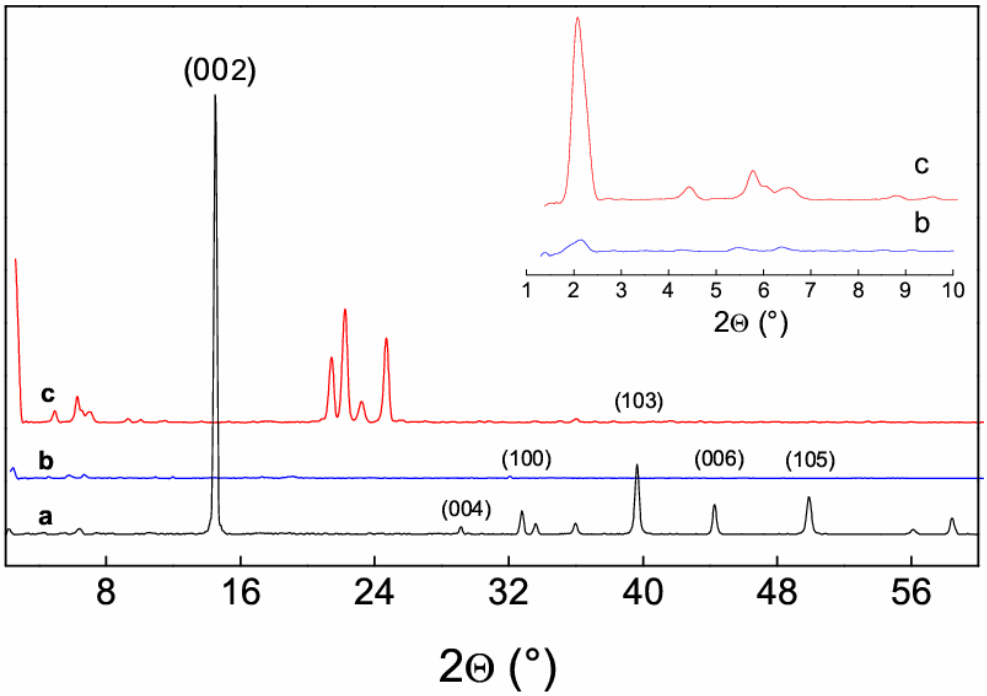

Fig. 3. X-ray powder diffraction patterns for the nanocomposite products (a) MoS_2 (b) the nanocomposite product after hydrothermal treatment (HT) (c) hexadecylamine (HDA) surfactant. *Insert* Corresponding X-ray patterns acquired between double angles of 1.3−10°.

to definitively report any obvious decomposition of the MoS_2 due to conditions of the HT.

The XRD data shows that the phase of the post-HT product is coincident with that of the amines and secondly, that the MoS_2 is rearranged in a structure that exhibits characteristics of an amorphous phase. Another possibility that is currently being investigated is that the MoS_2 was oxidized to alkyl ammonium molybdate with a subsequent loss of weight due to the presence of excess oxygen during HT, but this remains to be conclusively verified and further work is currently being conducted to elucidate the exact coordination.

3.2 Thermogravimetric Analysis

Thermal stability measurements were determined using thermogravimetric analysis (TGA) and differential scanning calorimetry (DSC) for the compounds $Li_{0.1}MoS_2(HDA)_2$, $Li_{0.1}MoS_2(ODA)_{2.1}$ and their respective alkyl amine surfactants.

The corresponding TGA and DSC curves of the surfactants and the lamellar products $Li_{0.1}MoS_2(HDA)_2$ and $Li_{0.1}MoS_2(ODA)_{2.1}$ are shown in Fig. 4.

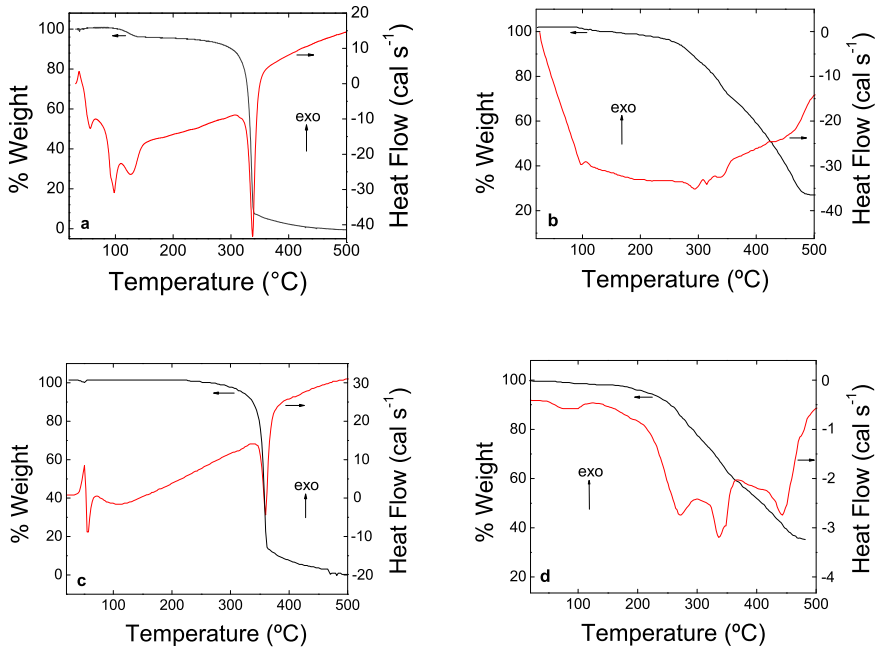

Fig. 4. Thermogravimetric analysis curves (TGA) and differential scanning calorimetric curves (DSC) of the products (a) HDA and (b) $Li_{0.1}MoS_2(HDA)_2$ (c) ODA and (d) $Li_{0.1}MoS_2(ODA)_{2.1}$.

Compound	Melting Point	Temp. Range	Max. Temp.	Thermal Effect
HDA	46	30 - 200	60, 100, 120	Endo
		200 - 400	338	
		400 - 500		
$Li_{0.1}MoS_2(HDA)_2$		30 - 200	100	Endo
		275 - 357	228, 314, 340	
		424 - 500	446	
ODA	54	30 - 200	54, 110	Endo
		200 - 400	359	
		400 - 500		
$Li_{0.1}MoS_2(ODA)_{2.1}$		30 - 200	80, 101, 119	
		200 - 400	292, 340	Endo
		400 - 510	442	

Table 1
Results of the differential scanning calorimetry (DSC) of the intercalated compounds. All temperatures are in degrees Celcius.

Compound	% (mol amine/mol MoS_2)	
	Elemental Analysis	TGA
$Li_{0.1}MoS_2(HDA)_2$	71.5	73.4
	(2.1)	(2.2)
$Li_{0.1}MoS_2(ODA)_{2.1}$	74.9	72.7
	(2.0)	(2.1)

Table 2
Comparison of results obtained from elemental analysis and thermal analysis for the nanocomposites. The percent uncertainty in the measurements is shown in parentheses.

The temperature range of decomposition of the nanocomposite occurred in three specific intervals and details are outlined in Table 1. In the first region (25−200°C) endothermic fusion peaks in the DSC curves of the nanocomposite shown in Fig. 4b and 4d are not observed due to the presence of the amines. The overall response is similar to that of the corresponding alkyl amine surfactant, shown in Figs 4a and 4c (HDA 46°C, ODA 54°C). There is a clear indication, however, that all the amine is contained within the intercalated compound as three distinct peaks are observed in the DSC curves shown in Figs 4b and 4d attributed to melting of the amine and the vaporization of any water present in the host-guest matrix.

The second interval of temperature (200−400°C) exhibits several characteristic peaks for the endothermic decomposition of the nanocomposite. Although the accurate assignation of specific processes in this interval is relatively difficult, the endothermic processes are due primarily to the strong binding of the amine in the organic-inorganic compound interlaminar spacing. In the case of the alkyl amine (Figs 4a and 4c), the TGA curves show a progressive weight loss in a similar range of temperature with a maximum for HDA observed at 338°C and for ODA at 359°C. These characteristic temperature values correspond to the boiling points of these compounds.

The third interval (400−550°C) shows the decomposition of the guest in the case of the nanocomposite with a 73% of weight loss in $Li_{0.1}MoS_2(HDA)_2$ and 72% for $Li_{0.1}MoS_2(ODA)_{2.1}$. The stoichiometry of the intercalated compounds is corroborated by the near-equivalence between the results of thermal analysis and elemental analysis of the intercalated compounds, and details are outlined in Table 2. The results of the TGA analysis in the range 40−500°C (Tables 1 and 2) of the pure amines and the series of compounds $Li_xMoS_2(C_nH_{2n+1}NH_2)_y$ show that the decomposition and weight loss of the alkyl amines occurs in a smaller range of temperature to that of the nanocomposite and that the decomposition is not progressive.

The lamellar product $Li_{0.1}MoS_2(HDA)_2$ used during HT exhibits a high degree of lamellar order. TEM was employed to examine the organic/inorganic lamellar nanocomposite product after HT and a typical example is shown in Fig. 5a where a coiled or plait-like structure is observed. Such examination was conducted using maximum accelerating voltage of 100 kV and during image acquisition, no degradation of the structures was observed due to the electron beam.

The nanocoil structure, however, does not have a hollow center, but displays areas of high diffraction contrast. The corresponding electron diffraction of the coiled structure exhibits some degree of crystallinity. Indexation of the electron diffraction pattern (Fig. 5a inset) is consistent with the MoS_2 hexagonal phase. The interlamellar distances to corresponding to the observed {105}, {008}, and {116} planes are 0.186 nm, 0.151 nm, and 0.124 nm, respectively, in good agreement with related observations [25]. Thus, the dark areas are the inorganic compound and the brighter areas are organic surfactant.

Under certain HT conditions these nanocoil structures are formed by the cross-over or interweaving of several organic/inorganic layers and result in a plait-like shape. Furthermore, the individual 'strings' of hexadecylamine/MoS_2 have typical outer diameters of $\sim$60$-$70 nm. The morphology of the nanocoils shows that the cylindrical 'strings' of MoS_2 (dark areas) exhibit a granular periodicity of $\sim$20 nm, over 30 times greater that the {002} plane of MoS_2. These cracks are perpendicular to the longitudinal axis of the each cylinder.

It is well known that in certain cases the HT of surfactant-mediated lamellar structures causes a rolling-up mechanism to occur [18]. In the case of the lithiated MoS_2 lamellar product, rolling of the lamella was observed resulting in the formation of a nanotubular structure. A typical TEM micrograph of the rolled-up MoS_2 nanotube is shown in Fig. 5b and the upper left TEM image shows a relatively low magnification micrograph of the nanotubes where their typical length is in the range 2 to 12 μm. The lower inset micrograph shows a magnified image of the coaxial tube morphology caused by rolling of the lamina during HT. The nanotubes have characteristic tubular dimensions of $\sim$25$-$100 nm (inner tube diameter) and $\sim$200$-$450 nm (outer tube diameter). The individual nanotubes tend to have lengths in the range 2$-$12 μm, depending on the size of individual exfoliated lamellar structures prior to HT. Efforts to accurately explain the mechanism of formation of these surfactant-mediated MoS_2 nanostructures are ongoing [24].

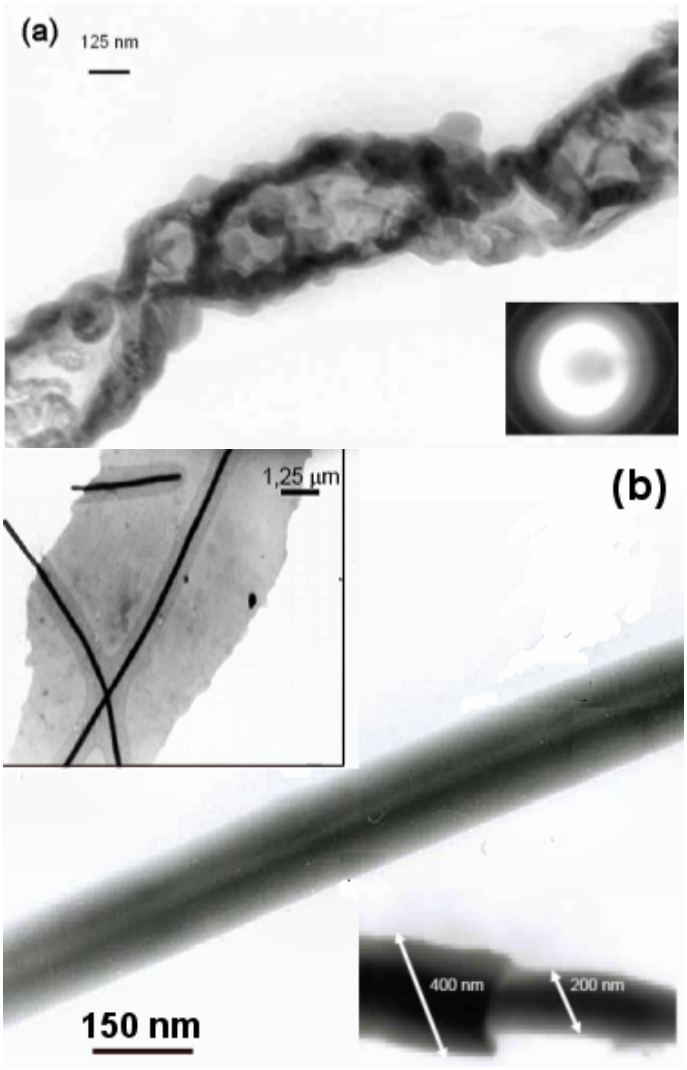

Fig. 5. Bright-field through-focal TEM micrograph of (a) the nanocoils of HDA/MoS_2. *Inset* Corresponding electron diffraction pattern (b) HDA/MoS_2 nanotubes. The nanotubes were observed to have outer diameters of 200−450 nm and inner diameters typically in the range ∼25−100 nm. *Inset Left* Lower magnification TEM micrograph highlighting the high aspect ratio of the nanotubes. *Inset Right* Coaxial rolled lamina of MoS_2 at the initial stage of nanotube formation by the 'rolling-up' mechanism.

4 Conclusions

We have demonstrated that organic-inorganic lamellar products based on the intercalation of amine in MoS_2 produces MoS_2 nanotubes and nanocoils. The pre-HT compound exhibits a high degree of crystallinity although the X-ray diffraction not allow definitive clarification of the phase of the post-HT nanotubes due to the organic-inorganic material rearranges to a structure that exhibits characteristics of a phase with a low degree of crystallinity. The ther-

mogravimetric analysis of these products corroborates the stoichiometry of the lamellar compounds. The MoS_2 nanotubes form during HT by rolling of amine-intercalated $LiMoS_2$ lamella and range in length from 2 to 12 μm. The nanotubes have typical inner diameter of hollow core of $\sim$25$-$100 nm while the their outer diameter ranges from 200 to 450 nm.

Although oxidation of the nanocomposite due to the conditions of hydrothermal treatment cannot be ruled out, the evidence suggests that the formation of the much less commonly observed nanocoils by interweaving of individual and separate 'strings' of organic and inorganic compounds, is due to the HT conditions. A self-assembly process similar to that observed for other inorganic nanostructure formation, is observed to occur during formation of MoS_2 nanotubular products.

Acknowledgements

The support of the Science Foundation Ireland (SFI), FONDECyT (Grants 1050344, 1030102, 7050081) are gratefully acknowledged. N. M. is grateful for a doctoral scholarship from Deutscher Akademischer Austauschdienst (DAAD). The authors also acknowledge the technical assistance of Mr Victor Monasterio.

References

[1] R. Tenne, L. Margulis, M. Genut, G. Hodes, Nature 360 (1992) 444.

[2] M. H. A. Hassan, Science 309 (2005) 65.

[3] (a) M. Remskar, Z. Skraba, R. Sanjines, Appl. Phys. Lett. 69 (1996) 351. (b) M. Remskar, A. Mrzel, Current Opinion in Solid State and Materials Science 8 (2004) 121.

[4] D. H. Kerridge, S. J. Walker, J. Inorg. Nucl. Chem. 39 (1977) 1579.

[5] Y. Tian, Y. He, Y. Zhu, Mater. Chem. Phys. 87 (2004) 87.

[6] M. Chhowalla, G. A. J. Amaratunga, Nature 407 (2000) 164.

[7] R. Rothschild, S. R. Cohen, R. Tenne, Appl. Phys. Lett. 75 (1999) 4025. (b) J. Chen, N. Kuriyama, H. T. Yuan, H. T. Takeshita, T. Sakai, J. Am. Chem. Soc. 123 (2001) 11813.

[8] V. Nemanic, M. Zumer, B. Zajec, J. Pahor, M. Remskar, A. Mrzel, P. Pajan, D. Mihalovic, Appl, Phys. Lett. 82 (2003) 4573.

[9] D. Mihailovic, Z. Jaglicic, R. Dominko, A. Omerzu, A. Mzrel, J. Phys. Chem. Solids. 64 (2004) 707.

[10] R. Dominko, M. Gaberscek, D. Arcon, A. Mrzel, M. Remskar, D. Mihailovic, S. Pejovnik, J. Jammink, Electrochim. Acta 48 (2003) 3079.

[11] J. Chen, S. L. Li, Z. L. Tao, J. Alloys and Compounds, 356 (2003) 413.

[12] J. Goldberg, R. Fan, P. Yang, Acc. Chem. Res. 39 (2006) 239.

[13] M. Nath, A. Govindarai, C. N. R. Rao, Adv. Mater. 13 (2001) 283.

[14] M. Remskar, A. Mrzel, Z. Skraba, A. Jesih, M. Ceh, J. Demsar, P. Stadelmann, F. Levy, D. Mihailovic, Science 292 (2001) 479.

[15] J. Chen, S. L. Li, Q. Xu, K. Tanaka, Chem. Commun. 16 (2002) 1722.

[16] E. Benavente, M. A. Santa Ana, F. Mendizábal, G. González, Coord. Chem. Rev. 224 (2002) 87.

[17] V. Lavayen, C. O'Dwyer, M. A. Santa Ana, N. Mirabal, E. Benavente, G. Cárdenas, G. González, and C. M. Sotomayor Torres, Appl. Surf. Sci. (2006), doi:10.1016/j.apsusc.2006.07.039.

[18] C. O'Dwyer, D. Navas, V. Lavayen, E. Benavente, M. A. Santa Ana, G. González, S. B. Newcomb, C. M. Sotomayor Torres, Chem. Mater. 18 (2006) 3016.

[19] V. Sanchez, E. Benavente, V. Lavayen, C. O'Dwyer, C. M. Sotomayor Torres, G. González and M. A. Santa Ana, Appl. Surf. Sci. (2006), doi:10.1016/j.apsusc.2005.10.011.

[20] G. González, M. A. Santa Ana, E. Benavente, V. Sánchez, N. Mirabal, Mol. Cryst. Liq. Cryst. 374 (2002) 229.

[21] V. Sánchez, E. Benavente, M. A. Santa Ana, G. González, Chem. Mater. 11 (1999) 2296.

[22] D. Demus, J. Gooby, G. W. Gray, H. W. Spiess, V. Vill, Handbook of Liquid Crystals, Wiley-VCH, Weinheim, 1998.

[23] N. Mirabal, V. Lavayen, E. Benavente, M. A. Santa Ana, G. González, Microelectronics Journal 35 (2004) 37.

[24] V. Lavayen, N. Mirabal, M. A. Santa Ana, E. Benavente, C. M. Sotomayor-Torres, G. González, in preparation, 2006.

[25] Q. Li, J. T. Newberg, E. C. Walter, J. C. Hemminger, R. M. Penner, Nano Lett. 4 (2004) 277.